DARK MATTER CONSTRAINTS WITH THE FIRST YEAR OF FERMI-LAT DATA

T. YLINEN[†,a] and E. NUSS[‡],
on behalf of the Fermi-LAT Collaboration
[†]*Department of Physics, Royal Institute of Technology, AlbaNova University Center, SE-106 91 Stockholm, Sweden - School of Pure and Applied Natural Sciences, University of Kalmar, SE-391 82 Kalmar, Sweden - The Oskar Klein Centre for Cosmoparticle Physics, AlbaNova University Center, SE-106 91 Stockholm, Sweden*
[‡]*Laboratoire de Physique Théorique et Astroparticules, Université Montpellier 2, CNRS/IN2P3, Montpellier, France*

Our understanding of the Universe today includes overwhelming observational evidence for the existence of an elusive form of matter that is generally referred to as dark. Although many theories have been developed to describe its nature, very little is actually known about its properties. The launch of the Fermi Gamma-ray Space Telescope in 2008 opened a new window for the indirect experimental search for dark matter through high-energy gamma-rays. The principal instrument onboard, the Large Area Telescope (LAT), is designed to measure gamma-rays with energies ranging from 20 MeV to more than 300 GeV. The first year of *Fermi*-LAT data has allowed for a large variety of dark matter searches and we present here a review of the results from the different analyses.

1 Introduction

The existence of dark matter (DM) was first proposed already in 1933 by Zwicky [1], after studying the radial velocities of eight galaxies in the Coma galaxy cluster. The observed velocity dispersion was unexpectedly large, which suggested additional matter that was non-luminous (so-called "dark" hereafter). A large variety of observations supporting the existence of such matter have been performed since then and relate to the Big Bang Nucleosynthesis (BBN) [2], gravitational lensing [3] and the cosmic microwave background (CMB) [4]. The most visual evidence of DM to date comes from the merging galaxy cluster 1E 0657-558 ("Bullet Cluster"), where a clear separation of the mass (determined from gravitational lensing) and the X-ray emitting plasma can be seen [5].

Combined, these observations have constrained the fractions of the energy density in the Universe in the form of matter and in the form of a cosmological constant to $\Omega_M \sim 0.3$ and $\Omega_\Lambda \sim 0.7$, respectively, with ordinary baryonic matter only constituting about $\Omega_B \sim 0.05$ [6]. Non-baryonic matter therefore seems to be the dominating form of matter in the Universe.

A favored model of the Universe that is in reasonable agreement with observations is the so-called ΛCDM model, which features long-lived and collisionless Cold Dark Matter (CDM) and a contribution from a cosmological constant (Λ).

[a]Speaker

A potential candidate for the CDM, that naturally provides the correct present-day relic abundance of DM, are Weakly Interacting Massive Particles (WIMPs). These are thought to annihilate or decay into Standard Model particles and one of the possible resulting particles are gamma-rays. These gamma-rays can be categorized into continuum signals and spectral line signals, which are produced mainly through the decay of neutral pions created in the hadronization of e.g. quark-antiquark final states and via loop-suppressed channels directly into monochromatic gamma-rays, respectively.

Continuum signals represent excesses in the overall energy spectrum that can not be accounted for by the existing components, which include the diffuse galactic emission, the isotropic diffuse emission and point sources. This type of search is limited by the precision to which the existing components can be described.

Many viable DM candidates can also give rise to spectral lines via annihilation or decay channels directly into monochromatic gamma-rays. The final state then constitutes one gamma-ray and some other particle X with a mass of M_X, which can e.g. be another gamma-ray, a Z-boson, a Higgs boson, a neutrino or a non-Standard Model particle. The photon energy E_γ, produced in a non-relativistic annihilation process, is then given by the equation $E_\gamma = M_\chi \left(1 - M_X^2/4M_\chi^2\right)$, where M_χ is the mass of the DM particle. The corresponding equation for decays is provided by the substitution $M_\chi \rightarrow M_\chi/2$.

An observation of a spectral line would be a "smoking-gun" for DM, since no other astrophysical process should be able to produce it. However, many models also predict either low branching fractions or low cross-sections for those channels, which means that a halo with a large central concentration, the existence of substructure that boosts the signal or the Sommerfeld enhancement [7] might be needed to be able to observe the signal.

The distribution of DM on galactic and sub-galactic scales is currently still a matter of debate but plays an important role in the detection of DM signals. A phenomenological halo density profile is generally used to describe most of the observed rotation curves of galaxies and it is based on N-body simulations. This smooth and spherically symmetric profile is given by Eq. 1,

$$\rho(r) = \frac{\delta_c \rho_c}{(r/r_s)^\gamma \left[1 + (r/r_s)^\alpha\right]^{(\beta-\gamma)/\alpha}}, \tag{1}$$

where r is the angular radius from the galactic center, r_s is a scale radius, δ_c is a characteristic dimensionless density, and $\rho_c = 3H^2/8\pi G$ is the critical density for closure. A variety of halo profiles following this equation exist and differ in the values of the (α,β,γ) parameters. Two examples of profiles that are commonly used are the Navarro, Frenk and White (NFW) model with (1,3,1) [8] and the isothermal profile with (2,2,0) [9]. Another halo profile, which is observationally favored, is the Einasto profile [10,11]. The Einasto profile takes the form as given in Eq. 2,

$$\rho_{Einasto}(r) = \rho_s e^{-(2/a)[(r/r_s)^a - 1]}, \tag{2}$$

where ρ_s is the core density and a is a shape parameter.

For a specified halo profile, the total energy-dependent flux of gamma-rays from annihilating DM is the sum of the fluxes from the different final states of branching fraction B_f and depends on the mass of the DM particle, the velocity-averaged cross-section $\langle\sigma v\rangle$, the solid angle Ω of the observed region-of-interest and the integral of the square of the halo profile over the line-of-sight according to Eq. 3.

$$\frac{d\Phi}{dE_\gamma}(E_\gamma, \phi, \theta) = \frac{1}{4\pi} \frac{\langle\sigma v\rangle}{2M_\chi^2} \sum_f \frac{dN_\gamma^f}{dE_\gamma} B_f \times \int_{\Delta\Omega(\phi,\theta)} d\Omega' \int_{\mathrm{LoS}} \rho^2\left(\vec{r}\left(l, \phi', \theta'\right)\right) dl \tag{3}$$

In the extragalactic case, the flux is the integrated flux from all redshifts. The equation above therefore also depends on the optical depth, which governs the absorption, an assumed model for the enhancement of the annihilation signal due to substructure and the parametrization of the energy content in the Universe.

2 Fermi Large Area Telescope

The Fermi Gamma-ray Space Telescope (also called *Fermi*), was successfully launched on a Delta II heavy launch vehicle from Cape Canaveral in Florida, USA, on June 11, 2008. The satellite was formerly known as the Gamma-ray Large Area Space Telescope (GLAST) but was renamed after its launch. The satellite orbits the Earth at an altitude of about 565 km and with an inclination angle of about 25.6°. One orbit takes about 90 minutes and full-sky coverage is reached in only two orbits. The satellite consists of two detector systems, the Large Area Telescope (LAT) and the Gamma-ray Burst Monitor (GBM).

The LAT covers the approximate energy range from 20 MeV to more than 300 GeV. The instrument is a pair-conversion telescope, designed to measure the electromagnetic showers of incident gamma-rays over a wide field-of-view while rejecting incident charged particles with an efficiency of 1 to 10^6. It consists of a 4 x 4 array of 16 identical modules on a low-mass structure. Each of the modules has a gamma-ray converter tracker for determining the direction of the incoming gamma-ray and a calorimeter for measuring its energy. The tracker array is surrounded by a segmented anti-coincidence detector. In addition, the whole LAT is shielded by a thermal-blanket micro-meteoroid shield.

The performance and sensitivity of the LAT are unprecedented. The field of view is $\sim$2.4 sr (at 1 GeV), the effective area $>$ 1 GeV is $\sim$8000 cm^2 on-axis and the energy resolution is $<$15% at energies $>$100 MeV.

3 Dark matter searches

The *Fermi*-LAT instrument allows for a large variety of searches for dark matter in the gamma-ray region. The sensitivity of such searches, however, depends on the spatial region selected for the search. Any region has its advantages and disadvantages. Although the galactic center region has fairly large photon statistics, it is affected by source confusion and a strong diffuse photon background. Alternative locations, which may give a better signal-to-noise ratio include for example dark matter satellites (substructures containing only dark matter), dwarf spheroidal galaxies (substructures with optical counterparts but with high mass-to-light ratios) and galaxy clusters at high galactic latitudes, where the photon background is lower and the source identification is better. The extragalactic background has large photon statistics, but is limited by astrophysical uncertainties.

We present here the results from all dark matter searches performed by the *Fermi*-LAT Collaboration after one year of observations.

3.1 Clusters of galaxies

Clusters of galaxies are a distant source type but they are dark matter dominated and typically at high galactic latitudes, which make them ideal targets for DM searches.

In this analysis, six clusters were selected from the HIghest X-ray FLUx Galaxy Cluster Sample (HIGFLUGCS) catalog and an unbinned likelihood fit with both spatial and spectral models was performed. No significant gamma-ray emission was, however, detected from the selected clusters for 11 months of data [12]. Assuming an NFW profile, the upper limits at 95%

confidence level, shown in Fig. 1, begin to constrain the allowed phase space, especially for models where the results from the PAMELA experiment are interpreted in terms of DM annihilations.

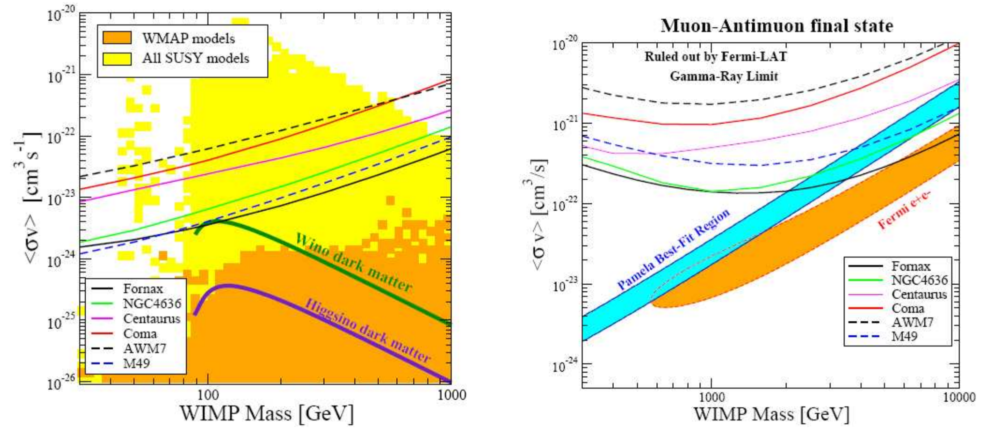

Figure 1: Upper limits at 95% confidence level for cluster of galaxies and for assumed $b\bar{b}$ (*left*) and $\mu^+\mu^-$ final states (*right*) [12].

3.2 Cosmological dark matter

The search for cosmological DM includes the contribution from DM from all halos at all redshifts. The search is based on the measured isotropic diffuse gamma-ray background emission [13] and a number of cases have been considered. These include 4 annihilation clustering enhancement models, 3 particle physics models for dark matter, 2 absorption models and 2 upper limit calculations (conservative and stringent). For more details, see [14]. As can be seen in Fig. 2, the upper limits can be very constraining for some cases. However, there are large uncertainties in the modeling of the evolution of DM structure and substructure as well as in the estimation of the isotropic background, which make the interpretation more challenging.

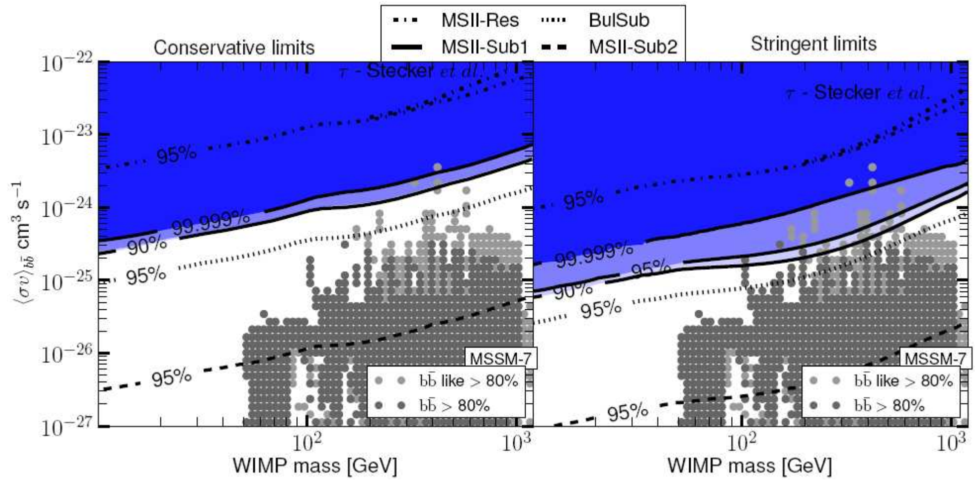

Figure 2: Upper limits for cosmological dark matter for an assumed $b\bar{b}$ final state in the conservative (*left*) and stringent (*right*) case [14].

3.3 Galactic center

The galactic center (GC) coincides with the cusped part of the theorized DM halo density profile, which is expected to be the strongest source of gamma-rays from DM annihilations.

The literature devoted to the possible signatures from DM in the gamma-ray region at the GC is extensive. The vicinity of the GC, however, also constitutes the most violent and active region of our galaxy and harbors numerous objects capable of accelerating cosmic rays to very high energies. The resulting gamma-rays are produced by inverse Compton scattering of electrons or pion decays following from e.g. proton-proton interactions.

A bright and very high energy gamma-ray point source has been observed by several other experiments and it is now widely considered to be a standard astrophysical source associated either with the bright compact radio source Sgr A* or with the candidate pulsar wind nebula G359.95-0.04 [15]. This source is a formidable background for DM studies in this region.

In Fig. 3, a preliminary fit from the ongoing analysis of the GC region is shown [16]. The observed region is composed of the square $7° \times 7°$ around the GC and the modeled components include the galactic diffuse emission, based on GALPROP, the isotropic diffuse emission and point sources from the first *Fermi*-LAT catalog. As can be seen in the figure, the model mostly reproduces the data within the uncertainties, but a residual gamma-ray emission is left, not accounted for by the above model. However, the disentanglement of a potential DM signal requires a detailed understanding of the conventional astrophysics.

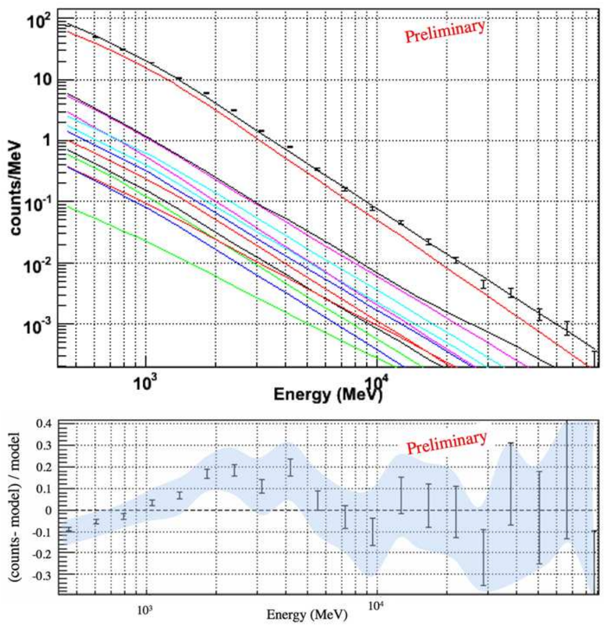

Figure 3: A preliminary fit (*top*) and residuals (*bottom*) to the gamma-rays from the galactic center region [16].

3.4 Dark matter subhalos

DM subhalos can be categorized into DM satellites and optically observed dwarf spheroidal galaxies. The former represent substructures that contain only DM. These may then shine in radiation from DM annihilations/decays. The analysis is at the time of writing still ongoing. However, preliminary results on 10 months of *Fermi*-LAT data include no detection of such structures.

The second category refer to low luminosity optically observed galaxies that are companions to a larger host galaxy. They are characterized by high mass-to-light ratios in the range 10-1000, which makes them dark matter dominated. Many of them are also nearby.

In the analysis, 14 dwarf spheroidal galaxies were selected, based on their proximity, galactic latitude and dark content as inferred from recent stellar velocity measurements [17]. A binned profile likelihood search on 11 months of *Fermi*-LAT data, assuming an NFW halo profile, was then performed. No gamma-ray excesses were, however, observed and 8 limits with DM densities inferred from stellar data were derived. As is shown in Fig. 4, the upper limits at 95% confidence level are beginning to constrain the mSUGRA, MSSM and AMSB parameter spaces.

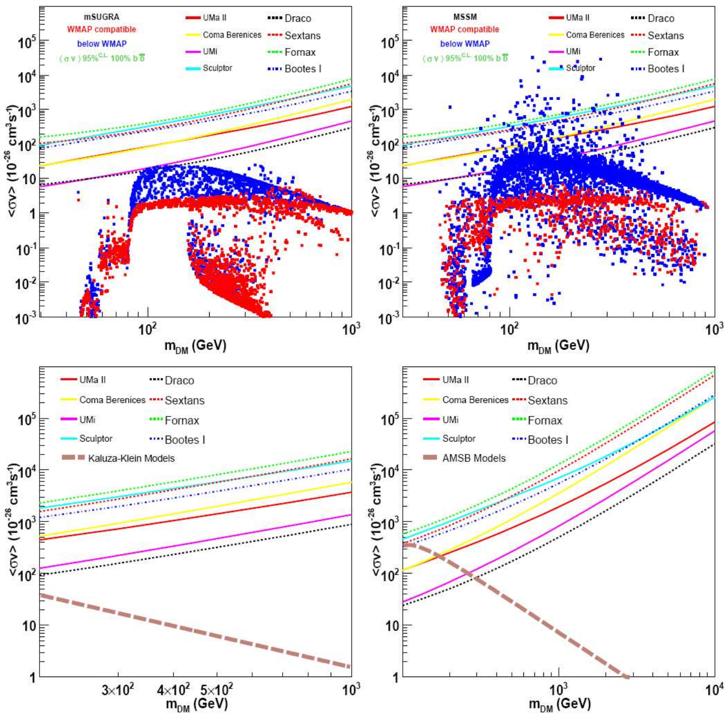

Figure 4: Upper limits at 95% confidence level as compared to mSUGRA, MSSM, Kaluza-Klein and AMSB parameter spaces using data from dwarf spheroidal galaxies with the *Fermi*-LAT [17].

A dedicated analysis on a specific dwarf spheroidal galaxy, Segue 1, has also been performed [18]. The analysis combines a binned likelihood analysis with CMSSM parameter scans via `DarkSUSY` using a nested sampling algorithm. However, the disfavoured models are already strongly disfavoured by relic density constraints.

3.5 Spectral lines

The search for spectral lines from dark matter consists of an unbinned fit to the data using the profile likelihood technique and can be used for both detection and upper limits. The likelihood model is constructed within the `RooFit` framework and requires an accurate modeling of the energy dispersion of the detector. These are determined from full detector simulations at specified energies and interpolations at intermediate energies. The data selection used for the spectral line search differs from standard analyses, since additional cuts with respect to the public data event class have been performed in order to reduce the charged particle contamination. In addition, the profile energy has been used instead of the standard energy.

The region-of-interest, chosen for this search, is defined by the sum of the regions $|b| > 10°$ and a square of $20° \times 20°$ around the galactic center. Point sources inherent in a preliminary point source catalog, corresponding to 11 months of *Fermi*-LAT data, were masked.

The search did not result in a detection and upper limits on the velocity-averaged cross-section and the decay lifetime at 95% confidence levels were calculated [19] as is shown in Fig. 5. These are still about a factor of 10 from the allowed MSSM and mSUGRA parameter spaces. However, the results disfavor, by a factor of 2–5, a model where the wino is the lightest supersymmetric particle [20]. At 170 GeV, the model predicts $\langle \sigma v \rangle_{\gamma Z} = 1.4 \times 10^{-26}$ cm^3 s^{-1}.

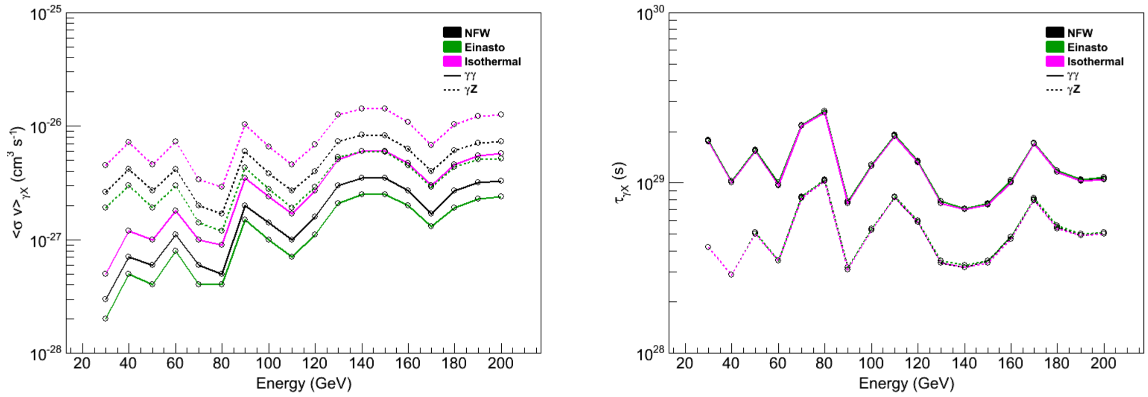

Figure 5: Upper limits at 95% confidence level on the cross-section (*left*) and the decay lifetime (*right*).

3.6 Electrons and positrons

The *Fermi*-LAT instrument can also be used to measure electrons and positrons, but the lack of a magnet prohibits the separation of the two. This kind of study is most relevant for cosmic-ray propagation models and the investigation of possible nearby sources, but a rejection power of 10^3–10^4 for protons is required. This is achieved via a separate series of trigger settings and cuts on detector variables.

The preliminary spectrum from combining a low-energy and high-energy analysis is shown in Fig. 6 in addition to an intermediate step in the analysis that shows the separation of electrons from hadrons for data and simulation [21]. The results indicate that any reasonable model (e.g. GALPROP), where a simple continuous distribution of sources is assumed, is not compatible with the measured spectrum.

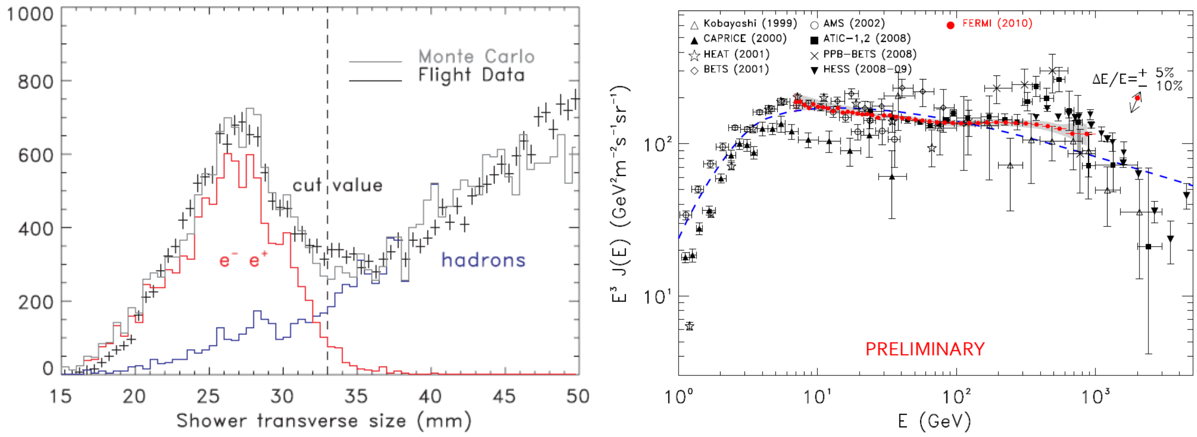

Figure 6: An intermediate step in the analysis chain (*left*) and preliminary electron-positron spectrum (*right*).

Many possible interpretations of the shape of the measured spectrum, in combination with the results from other experiments and measurements, have been suggested. These include e.g. nearby pulsars, source stochasticity and a revision of our understanding of cosmic-ray acceleration [22,23]. Although a DM contribution is not required to explain the measurements, it cannot be ruled out at this point either.

4 Summary and conclusions

Fermi Gamma-ray Space Telescope has opened a new era in DM searches and a large variety of analyses have been developed for clusters of galaxies, DM subhalos, cosmological DM and spectral lines. No significant detections have been made, but constraints that start to probe the available phase space have been put on the annihilation cross-section and decay lifetimes. In addition, several ongoing analyses are now being finalized, including studies of DM satellites and the complicated galactic center region. The *Fermi* mission is expected to continue for 5-10 years and the future therefore promises a plethora of interesting results.

Acknowledgments

The *Fermi*-LAT Collaboration acknowledges generous ongoing support from a number of agencies and institutes that have supported both the development and the operation of the LAT as well as scientific data analysis. These include the National Aeronautics and Space Administration and the Department of Energy in the United States, the Commissariat à l'Energie Atomique and the Centre National de la Recherche Scientifique / Institut National de Physique Nucléaire et de Physique des Particules in France, the Agenzia Spaziale Italiana and the Istituto Nazionale di Fisica Nucleare in Italy, the Ministry of Education, Culture, Sports, Science and Technology (MEXT), High Energy Accelerator Research Organization (KEK) and Japan Aerospace Exploration Agency (JAXA) in Japan, and the K. A. Wallenberg Foundation, the Swedish Research Council and the Swedish National Space Board in Sweden. Additional support for science analysis during the operations phase is gratefully acknowledged from the Istituto Nazionale di Astrofisica in Italy and the Centre National d'Études Spatiales in France.

References

1. F. Zwicky, *Helvetica Physica Acta* **6**, 110 (1933).
2. S. Sarkar, *Rep. Prog. Phy.* **59**, 1493 (1996).
3. J.A. Tyson, G.P. Kochanski & I.P. Dell'Antonio, *Astrophysical J.* **498**, L107 (1998).
4. D.N. Spergel, et al., *Astrophysical J. Suppl.* **170**, 377 (2007).
5. D. Clowe, et al., *Astrophysical J.* **648**, L109 (()2006).
6. P. Ullio, et al., *Phys. Rev.* D **66**, 12 (2002).
7. M. Lattanzi & J. Silk, *Phys. Rev.* D **79**, 083523 (2009).
8. J.F. Navarro, C.S. Frenk & S.D. White, *Astrophysical J.* **490**, 493 (1997).
9. J.N. Bahcall & R.M. Soneira, *Astrophysical J. Suppl.* **44**, 1980 (73).
10. J. Einasto, *Trudy Instituta Astrofiziki Alma-Ata* **5**, 87 (1965).
11. D. Merritt, et al., *Astrophysical J.* **132**, 2685 (2006).
12. A.A. Abdo, et al. (*Fermi*-LAT Collaboration), [arXiv:astro-ph/1002.2239] (2010).
13. A.A. Abdo, et al., (*Fermi*-LAT Collaboration), *Phys. Rev. Lett.* **104**, 101101 (2010).
14. A.A. Abdo, et al. (*Fermi*-LAT Collaboration), *J. Cosm. Astropart. Phys.* **04**, 014 (2010).
15. C. van Eldik, et al., (H.E.S.S. Collaboration), [arXiv:astro-ph/0709.3729] (2007).
16. V. Vitale & A. Morselli, (*Fermi*-LAT Collaboration), [arXiv:astro-ph/0912.3828] (2009).
17. A.A. Abdo, et al. (*Fermi*-LAT Collaboration), *Astrophysical J.* **712**, 147 (2010).
18. P. Scott, et al., *J. Cosm. Astropart. Phys.* **01**, 031 (2010).
19. A.A. Abdo, et al. (*Fermi*-LAT Collaboration), *Phys. Rev. Lett.* **104**, 091302 (2010).
20. G. Kane, R. Lu, & S. Watson, *Phys. Lett.* B **681**, 151 (2009).
21. A.A. Abdo, et al. (*Fermi*-LAT Collaboration), *Phys. Rev. Lett.* **102**, 181101 (2009).
22. D. Grasso, et al., *Astropart. Phys.* **32**, 140 (2009).
23. P. Blasi, *Phys. Rev. Lett.* **103**, 051104 (2009).